ANALYTIC MODEL OF THE ION ANGULAR DISTRIBUTION IN A COLLISIONAL SHEATH

by

V. Vahedi, R. A. Stewart, and M. A. Lieberman

Memorandum No. UCB/ERL M92/114

20 September 1992

ANALYTIC MODEL OF THE ION ANGULAR DISTRIBUTION IN A COLLISIONAL SHEATH

by

V. Vahedi, R. A. Stewart, and M. A. Lieberman

Memorandum No. UCB/ERL M92/114

20 September 1992

ELECTRONICS RESEARCH LABORATORY

College of Engineering
University of California, Berkeley
94720

ANALYTIC MODEL OF THE ION ANGULAR DISTRIBUTION IN A COLLISIONAL SHEATH

by

V. Vahedi, R. A. Stewart, and M. A. Lieberman

Memorandum No. UCB/ERL M92/114

20 September 1992

ELECTRONICS RESEARCH LABORATORY

College of Engineering
University of California, Berkeley
94720

Analytic Model of the Ion Angular Distribution in a Collisional Sheath

V. Vahedi, R. A. Stewart, and M. A. Lieberman
Department of Electrical Engineering and Computer Science
and the Electronics Research Laboratory,
University of California, Berkeley
Berkeley, CA 94720

Abstract

An analytic model is developed for the ion angular distribution in a collisional sheath. In a previous study, the one-dimensional (normal to the sheath) ion velocity distribution was obtained under the assumption that charge-exchange is the dominant ion-neutral collision mechanism. In the present model, we assume $\lambda_{scat} > \lambda_{cx}$, where λ_{scat} and λ_{cx} are the mean free paths for ion-neutral elastic scattering and charge-exchange collisions, respectively. With this assumption, the angular distribution mainly arises from ions that strike the electrode after undergoing only one scattering collision following the last charge-exchange collision. Comparison of the analytic model with results obtained from a particle-in-cell simulation gives excellent agreement. Both the average angle of ions striking the electrode and the ratio of parallel to perpendicular ion flux at the electrode are shown to scale with the ratio of scattering to charge-exchange cross-sections, $\sigma_{scat}/\sigma_{cx}$.

1 Introduction

With decreasing feature sizes in IC design, process tolerances are becoming increasingly more stringent. Plasma etching processes must minimize undercut in achieving an anisotropic etch, particularly in trench structures. The proposed Plasma Immersion Ion Implantation (PIII) trench doping for DRAMs requires a nearly uniform sidewall and trench-bottom profile. Control of the above process necessitates an understanding of the directionality of ion transport in the sheath.

The effect of collisions on ion sheath dynamics has been studied for many years in an attempt to accurately predict both the energy and angular distribution of ions bombarding a surface [1-14].

These studies have made use of varying levels of modeling complexity and accuracy. The most physically detailed modeling technique is the Monte Carlo method [1-4]. This method allows for accurate treatment of collisions, and may be solved self-consistently with Poisson's equation [14] [15] [16]. The disadvantage of this method is that it is computationally intensive.

Several self-consistent kinetic models have been developed for describing ion sheath dynamics[5-9]. These models require solving coupled non-linear differential equations, and often necessitate using a simple collision model to obtain a solution.

For the purpose of predicting the sensitivity and scaling of the anisotropy with controllable process parameters, analytical models are very desirable. Such models also provide an improved understanding of ion transport physics. While analytical models often contain several simplifying assumptions, compared to Monte Carlo or kinetic approaches, they may be used with good accuracy in some range of operating conditions. Furthermore, with the availability of Monte Carlo simulation results (or experimental measurements) the accuracy of analytical models can be verified.

One of the earliest analytical models of sheath dynamics was that of Davis and Vanderslice [10]. In their model, they considered only charge transfer collisions, hence only the one-dimensional energy distribution function at the electrode could be obtained. Vahedi *et al.* [16], proposed a similar analytical model and demonstrated good agreement with Monte Carlo simulation results for the energy distribution function. In the present work, we extend the work of Vahedi *et al.* to include the effect of elastic scattering in order to obtain the angular distribution of ions at the electrode. Under the assumption that charge exchange is the dominant scattering mechanism, elastic scattering is treated perturbatively by assuming that (1) ions strike the electrode after undergoing at most one scattering collision following the last charge exchange collision, and (2) the ion velocity distribution prior to the scattering event is due only to charge exchange collisions. Comparisons with Monte Carlo simulations are made and an application to trench profiles is considered.

2 Assumptions

The assumptions in the model are:

(1) The DC sheath voltage is much larger than the electron temperature in the bulk plasma, ($V_0 \gg T_e$), as seen in Fig. 1, hence $s \gg \lambda_{De}$ where s is the sheath width and λ_{De} is the electron Debye length.

(2) The electron density in the sheath is assumed to be zero, $n_e = 0$.

(3) The ion density in the sheath is uniform in space [16] as shown in Fig. 1 (linear electric field approximation).

(4) The ion motion is collisional; thus $s \gg \lambda_T$, where λ_T is the total ion-neutral mean free path.

(5) Ions undergo both charge-exchange and scattering collisions with neutral atoms with the assumption $\lambda_{scat} > \lambda_{cx}$, where λ_{scat} and λ_{cx} are the scattering and charge-exchange mean free paths.

(6) In a charge exchange collision, ions lose all their energy; hence the angular distribution is determined by the ion motion following the last charge-exchange collision prior to striking the target.

(7) Ions scatter only once following the last charge-exchange collision since $\lambda_{scat} > \lambda_{cx}$.

(8) The charge-exchange and scattering collision cross-sections are independent of ion energy (cross sections are typically flat over the energy range of interest 1-100 eV [17]). This assumption makes the computations more convenient but is not critical.

3 Analysis

Using the preceding assumptions to solve for the DC sheath potential, ϕ, from Poisson's equation, $d^2\phi/dz^2 = -en_s/\epsilon_0$ with $\phi(0) = -V_0$ and $\phi(s) = 0$, we obtain:

$$\phi(z) = -V_0(z-s)^2/s^2\,,$$

and define

$$V(z) = \phi(z) - \phi(0)\,. \tag{1}$$

In a previous study by Vahedi *et al.* [16], the ion velocity distribution normal to the surface was obtained under the assumption that charge-exchange is the dominant ion-neutral collision mechanism. Here we use their result to obtain an expression for the velocity distribution of the incident ion flux at z, just before the scattering, as shown in Fig. 2. In steady state, this flux is proportional to the ion dose D ($D = \Gamma T$ where Γ is the flux and T is the time). The ion dose energy distribution at z after the last charge-exchange collision at z_0 (see Fig. 2) is:

$$D(u,z) = \frac{n_s s u}{u_{m0}^2} \exp\left(-\frac{s}{2\lambda_T}\frac{u^2}{u_{m0}^2}\right) \tag{2}$$

where λ_T is the total ion-neutral mean free path ($\lambda_T^{-1} = \lambda_{scat}^{-1} + \lambda_{cx}^{-1}$), u is the ion velocity normal to the surface, n_s is the ion density in the sheath, and $u_{m0}^2 = 2V_0/M$. The expression in Eq. (2)

is the ion dose only a few mean free paths away from the wall and shows no z dependence. Hence over the time period T, the differential incident flux at z prior to scattering is (see Fig. 3)

$$d\Gamma_{inc}(u,z) = \Gamma_0 g(u) du\,, \tag{3}$$

where Γ_0 is the total incident ion flux at z, and

$$g(u) = \frac{su}{\lambda_T u_{m0}^2} \exp(-\frac{s}{2\lambda_T}\frac{u^2}{u_{m0}^2})\,.$$

Note that

$$\Gamma_{inc} = \int_u d\Gamma_{inc}(u,z) = \Gamma_0 \int_u g(u) du = \Gamma_0\,.$$

The differential scattered flux in the interval $[z, z-dz]$, as shown in Fig. 3, is given by

$$d\Gamma_{scat} = d\Gamma_{inc} n_0 \sigma_{scat}\, dz = \Gamma_0 g(u) du n_0 \sigma_{scat}\, dz\,, \tag{4}$$

where n_0 is neutral density and σ_{scat} is the scattering cross section. In order to find the ion flux scattered into (v,θ) we use:

(i) a transformation from u to (v,θ) such that

$$\int_v v dv \frac{\delta(v - f(u,\theta))}{v} = 1\,, \tag{5}$$

(ii) a differential cross section $I(\theta)$ which satisfies [17]

$$\sigma_{scat} = \int_\theta I(\theta) 2\pi \sin\theta d\theta\,. \tag{6}$$

The function f in Eq. (5) relates the scattered velocity v to the scattered angle θ and the incident normal velocity u, as seen in Fig. 2:

$$v = f(u,\theta)\,. \tag{7}$$

Inserting Eqs. (5) and (6) into Eq. (4), The differential scattered flux can now be written as

$$d\Gamma_{scat} = \int_v v dv \int_\theta d\theta d\Gamma_1(u,v,\theta)\,,$$

where

$$d\Gamma_1(u,v,\theta) = \Gamma_0 g(u) du\, n_0\, dz\, I(\theta) 2\pi \sin\theta \frac{\delta(v - f(u,\theta))}{v}\,. \tag{8}$$

Before finding the total scattered flux at z, we make the assumption that the ion-neutral scatterings are hard-sphere collisions. This allows us to define the differential cross-section $I(\theta)$ and the scattering function f in Eq. (7). Other types of scattering can be treated by defining the proper $I(\theta)$ and scattering function f. For hard-sphere collisions, the scattering function is [17]

$$v = f(u,\theta) = u\cos\theta\,,$$

and the differential cross-section becomes [17]

$$I(\theta) = \begin{cases} (\sigma_{scat}\cos\theta)/\pi & 0 \le \theta \le \pi/2\,, \\ 0 & \pi/2 \le \theta \le \pi\,. \end{cases} \tag{9}$$

Substituting the above expressions into Eq. (8), we get

$$d\Gamma_1(u,v,\theta) = \Gamma_0 g(u) du\, n_0\, \sigma_{scat}\, dz\, 2\sin\theta\cos\theta \frac{\delta(v - u\cos\theta)}{v}\,. \tag{10}$$

To find the total flux scattered in the interval $[z, z-dz]$, we must integrate Eq.(10) over all u's, that is:

$$\begin{aligned} \Gamma_1(v,\theta) &= \int_v d\Gamma_1(u,v,\theta) \\ &= \Gamma_0 n_0\, \sigma_{scat}\, dz \frac{2\sin\theta}{v} g(\frac{v}{\cos\theta})\,. \end{aligned} \tag{11}$$

This is the velocity and angular distribution of the ion flux at z. In order to determine an expression for the angular distribution of the ion flux at the target ($z = 0$), $\Gamma'(\theta')$, we make the following transformations, as shown in Fig. 2:

(a) $(v,\theta) \longrightarrow (v_y, v_z)$ where $v^2 = v_y^2 + v_z^2$ and $\theta = \tan^{-1}(v_y/v_z)$;

(b) $(v_y, v_z) \longrightarrow (v'_y, v'_z)$ where $v'_y = v_y$ and $v'^2_z = v_z^2 + 2V(z)/M$;

(c) $(v'_y, v'_z) \longrightarrow (v', \theta')$ where $v'_y = v'\sin\theta'$ and $v'_z = v'\cos\theta'$;

where $V(z)$ is defined in Eq. (1), and v_y is the transverse velocity.

We require that the total flux is conserved through the transformations. The total scattered flux arriving at the target ($z = 0$) can now be calculated to be:

$$\begin{aligned} \Gamma_{z=0} &= \int_z dz e^{-n_0\sigma_T z} \int_v v dv \int_\theta d\theta \Gamma_1(v,\theta) \\ &= \int_\theta d\theta' \int_{v'} v' dv' \int_z dz e^{-n_0\sigma_T z} \Gamma_2(v',\theta') \\ &= \int_0^{\pi/2} d\theta' \Gamma'(\theta')\,, \end{aligned}$$

where

$$\Gamma'(\theta') = \int_0^{u_{m0}\cos\theta'} v' dv' \int_0^{z_{max}(v',\theta')} dz e^{-n_0\sigma_T z} \Gamma_2(v',\theta')\,. \tag{12}$$

The exponential factor in Eq. (12) insures that ions undergoing scattering or charge-exchange collisions between position z and the target, $z = 0$, do not contribute to the ion flux at the target.

The flux $\Gamma_2(v',\theta')$ is obtained from transformations (a)-(c) to be:

$$\begin{aligned} \Gamma_2(v',\theta') &= \frac{2s\Gamma_0\sigma_{scat}}{\lambda_T u_{m0}^2} \frac{v'^2\sin\theta'\cos\theta'}{v'^2\cos^2\theta' - 2V(z)/M} \\ &\quad \times \exp\left(-\frac{s}{2\lambda_T u_{m0}^2} \frac{(v'^2 - 2V(z)/M)^2}{v'^2\cos^2\theta' - 2V(z)/M}\right)\,. \end{aligned} \tag{13}$$

The expression obtained in Eq. (12) is the angular distribution of the ions which suffered only one scattering collision after the last charge-exchange. These ions are the only ones contributing to the angular distribution; ions with multiple scatterings are disregarded. The expression for $\Gamma'(\theta')$ in Eq. (12) is a complicated integral which must be integrated numerically. The limits of integration for v' are trivial; however the upper limit in the z integration, $z_{max}(v', \theta')$, is somewhat complicated, thus the derivation of this quantity is considered in the appendix.

We can easily calculate the magnitude of the total scattered flux from Eq. (4) in terms of the total incident flux to be:

$$\begin{aligned} \Gamma_{scat} &= \int_0^{z_{max}} e^{-n_0 \sigma_T z} \int_u d\Gamma_{scat} \\ &= \frac{\sigma_{scat}}{\sigma_T}\Gamma_0, \qquad (z_{max} \gg \lambda_T). \end{aligned}$$

This expression allows us to rewrite $\Gamma'(\theta')$ in the form

$$\Gamma'(\theta') = \Gamma_0 \frac{\sigma_{scat}}{\sigma_T}\Gamma'_N(\theta'),$$

where $\Gamma'_N(\theta')$ is the normalized angular flux at the target.

We now define $< \theta_1 >$ as:

$$< \theta_1 >= \int_0^{\pi/2} d\theta' \theta' \Gamma_N(\theta') \tag{14}$$

the average angle of the ions striking the target after one scattering collision. If we assume $\sigma_T \gg \sigma_{scat}$, only a small fraction of the ions scatter and the rest arrive at the target with $\theta' = 0$, forming a delta function in the angular distribution at $\theta' = 0$. The total average angle of the ions arriving at the wall, $< \theta_T >$, is a weighted average of the scattered and unscattered ion fluxes:

$$\begin{aligned} < \theta_T > &= \frac{1}{\Gamma_0}\left(\int_0^{\pi/2} d\theta' \theta' \Gamma_{scat} + \int_0^{\pi/2} d\theta' \theta' \Gamma_{unscat}\right) \\ &= \frac{1}{\Gamma_0}\left(\frac{\sigma_{scat}}{\sigma_T}\Gamma_0 \int_0^{\pi/2} d\theta' \theta' \Gamma_N(\theta') + \frac{\sigma_{cx}}{\sigma_T}\Gamma_0 \int_0^{\pi/2} d\theta' \theta' \delta(\theta')\right) \\ &= \frac{\sigma_{scat}}{\sigma_T} \int_0^{\pi/2} d\theta' \theta' \Gamma_N(\theta') \\ &= \frac{\sigma_{scat}}{\sigma_T} < \theta_1 > \end{aligned} \tag{15}$$

Table 1 shows a few calculated parameters for several cases. The ion mass for all cases was chosen to be that of a proton. The DC sheath voltage, V_0, and the charge-exchange cross-section, σ_{cx} were held constant, while the gas pressure, p, and the ratio of charge-exchange to scattering cross-sections were varied. The sheath width s can be obtained from the results of Vahedi *et al.* [16]:

$$n_s = \frac{2\epsilon_0 V_0}{es^2},$$

where n_s is the ion density in the sheath. The same ion density was considered for all the cases, corresponding to a sheath width of 10 cm. The value of the sheath width was chosen to ensure that the ratio $\lambda_T/s \ll 1$, consistent with assumption (4). Equation (12) was numerically integrated to obtain the normalized angular distribution profile, $\Gamma_N(\theta')$, and compared with simulation results (See Sec. 4). Having calculated $\Gamma_N(\theta')$, we can then evaluate Eqs. (14) and (15) to get the average angle of the scattered and total ion fluxes. As shown in Table 1, the numerical integration results show that the average angle $< \theta_1 >$ of the scattered ions is typically 18-20 degrees and is essentially independent of both the gas pressure and the ratio $\sigma_{scat}/\sigma_{cx}$. Hence Eq. (15) provides a particularly simple scaling law. Although not shown in Table 1, the DC sheath voltage was also varied and no significant change was observed in $< \theta_1 >$. Since only the ratio V_0/M appears in the theory, this shows that $< \theta_1 >$ is also independent of M. The invariance of the average angle $< \theta_1 >$ can be explained by considering the average angle for hard-sphere scattering,

$$< \theta_{scat} >= \frac{\int_0^\pi \theta I(\theta) \sin\theta d\theta}{\int_0^\pi I(\theta) \sin\theta d\theta} = \frac{\pi}{8} = 22.5^\circ ,$$

where $I(\theta)$ is defined in Eq. (9). The average angle $< \theta_1 >$ is slightly less than $< \theta_{scat} >$ because of the acceleration from the scattering position to the wall. Furthermore, using the transformations (a)-(c) in Sec. 3, we obtain:

$$\begin{aligned} v'_y &= v_y \propto (V_0/M)^{1/2} , \\ v'_z &= \sqrt{v_z^2 + 2V(z)/M} \propto (V_0/M)^{1/2} , \end{aligned}$$

thus the scattered angle at the wall, $\theta' = \tan^{-1}(v'_y/v'_z)$, is independent of the ratio V_0/M. This result is valid for any scattering model in which Eq. (7) can be written in the form:

$$v = uf(\theta) .$$

Hence $< \theta_1 > \approx 20^\circ$, is a universal constant, for hard-sphere scattering and for $\lambda_T/s \ll 1$ and $\sigma_{scat}/\sigma_{cx} \ll 1$. For the cases where $\sigma_{cx} \gg \sigma_{scat}$ in Table 1, $< \theta_T >$ is typically less than one degree.

4 Comparison with simulation

The code PDP1 [14] [15] is used to simulate a bounded one-dimensional planar electrostatic plasma system. This code uses the particle-in-cell method, which is described in detail by Birdsall and Langdon [18], to solve for the particle and field parameters self-consistently. A Monte Carlo collision package has also been included to model charged particle-neutral interactions, such as ionization, excitation, momentum transfer, charge-exchange, and scattering collisions. The Monte Carlo package uses measured cross-sections to determine collision frequencies for various interactions.

In order to compare the analytic results obtained from numerical integration of Eq. (12) with the simulations, we consider both ion charge-exchange and scattering collisions in the simulations. The ion-neutral scatterings are assumed to be hard-sphere collisions in the simulation code. The simulation further assumes the scatterings to be isotropic collisions in the center-of-mass frame, which results in forward scatterings in the laboratory frame for equal ion-neutral masses [17]. The ion and neutral masses are chosen to be that of a proton, and the cross-sections are chosen to be constant over all energies for the purpose of comparison with the analytic model. A low-temperature plasma (T_e = 1 eV) is injected and recycled at the left boundary to simulate a semi-infinite plasma (see Fig. 1). The boundary condition on the right electrode is a large DC voltage (V_0 = 500V $\gg T_e$). A DC sheath is formed self-consistently, and the ions are found to be extracted according to a collisional Child's law [16] [19]. If the sheath width s, the DC voltage V_0, and the ion-neutral mean free path λ_i are set, one can determine the ion current density from the analytic model using the results of Vahedi *et al.* [16]:

$$J_i \propto (\frac{\lambda_i}{M})^{1/2} \frac{V_0^{3/2}}{s^{5/2}} . \tag{16}$$

If the ion current density is known, the left boundary condition can be adjusted to simulate only the DC ion sheath. To do this, the size of the system is set to be the sheath width, and ions only (no electrons) are injected at the left boundary at the current density obtained from Eq. (16). The right boundary condition is unchanged. This ion sheath simulation is identical to the usual ion-neutral Monte Carlo simulations, with the advantage of having a self-consistent electric field profile in the sheath.

The ion energy and angular profiles obtained from the semi-infinite plasma simulations were identical to those obtained from using the ion sheath simulation. The advantage of the ion sheath simulation is not having to resolve the electron motion, which plays no significant role in determining the ion profile at the target in a DC sheath.

Figures 4 and 5 show comparisons of numerical integration of Eq. (12) with the simulations for several cases listed in Table 1. The comparisons show excellent agreement in all cases even when the ratio $\sigma_{cx}/\sigma_{scat}$ is on the order of unity. More importantly, the simulation also verifies that the angular profile is a very weak function of neutral pressure and the cross-section ratio.

5 Application

We can use the results obtained from the analytic model to calculate the total ion flux parallel to and perpendicular to the wall, as shown in Fig. 6. The ion flux perpendicular to the wall is due to

the unscattered ions as well as the scattered ones:

$$\begin{aligned}\Gamma_z &= \int_0^{\pi/2} (\cos\theta' \Gamma_{scat} + \Gamma_{unscat}) d\theta' \\ &= \Gamma_0 \frac{\sigma_{scat}}{\sigma_T} \int_0^{\pi/2} \cos\theta' \Gamma_N(\theta') d\theta' + \Gamma_0 \frac{\sigma_{cx}}{\sigma_T} \\ &= \Gamma_0 \frac{\sigma_{scat}}{\sigma_T} < \cos\theta' > + \Gamma_0 \frac{\sigma_{cx}}{\sigma_T},\end{aligned}$$

where $< \cos\theta' >$ is the average value of $\cos\theta'$ over the angular profile. Unlike the perpendicular flux, only the scattered ions contribute to the parallel flux reaching the wall:

$$\begin{aligned}\Gamma_y &= \int_0^{\pi/2} \sin\theta' \Gamma_{scat} d\theta' \\ &= \Gamma_0 \frac{\sigma_{scat}}{\sigma_T} \int_0^{\pi/2} \sin\theta' \Gamma_N(\theta') d\theta' \\ &= \Gamma_0 \frac{\sigma_{scat}}{\sigma_T} < \sin\theta' >,\end{aligned}$$

where $< \sin\theta' >$ is the average value of $\sin\theta'$ over the angular profile. The ratio of these two fluxes is then:

$$\frac{\Gamma_y}{\Gamma_z} = \frac{< \sin\theta' >}{< \cos\theta' > + \sigma_{cx}/\sigma_{scat}} \tag{17}$$

The last column in Table 1 lists the calculated values for this flux ratio. In some cases this ratio can be as high as 13 percent. This is in fact the ratio of the ion flux that strikes the sidewalls of the trench to the flux that strikes the top and bottom of the trench. Note that for $\sigma_{cx} \gg \sigma_{scat}$,

$$\frac{\Gamma_y}{\Gamma_z} \approx \frac{\sigma_{scat}}{\sigma_{cx}} < \sin\theta' >,$$

where $< \sin\theta' >$ depends only weakly on the cross-section ratio, which is demonstrated in Table 1.

6 Conclusions

An analytical model has been developed for the angular distribution of ion flux at a target in a collisional sheath due to ion-neutral scattering collision, when charge-exchange is the dominant collision mechanism. The shape of the angular distribution function is found to be insensitive to variations in pressure and applied voltage and is in good agreement with PDP1 particle-in-cell simulations. The model predicts that the average angle of the ions arriving at a target after one scattering is typically 18-20 degrees. The average angle for all the ions, however is proportional to the ratio of charge-exchange to scattering cross-sections and is typically less than one degree when $\sigma_{scat} \ll \sigma_{cx}$.

7 Acknowledgement

This work was supported in part by a gift from Applied Materials, Inc. and a grant from the California Office of Competitive Technology, the state of California MICRO program, and a grant from the National Science Foundation.

A Appendix

The expression for $z_{max}(v', \theta')$ can be obtained by considering the transformation from (z, v, θ), to (z, v', θ') in Eq. (12) and the equations directly preceeding it. To do this, we obtain the extremum surface in (z, v, θ) and transform to (z, v', θ'). The maximum value of $v(z, \theta)$ is obtained when $u = u_m(z)$ is a maximum, *i.e.*,

$$\frac{1}{2} M u_m^2(z) = \phi(s) - \phi(z) ,$$

or

$$u_m(z) = u_{m0}(1 - z/s) . \tag{A1}$$

Hence the extremum surface in (z, v, θ) is

$$v = u_m(z) \cos\theta . \tag{A2}$$

Using the transformations (a)-(c) in Sec. 3, we obtain:

$$v = (v'^2 - 2V(z)/M)^{1/2} , \tag{A3}$$

and

$$\tan\theta = \frac{v' \sin\theta'}{(v'^2 \cos^2\theta' - 2V(z)/M)^{1/2}} ,$$

which leads to

$$\cos\theta = \frac{(v'^2 \cos^2\theta' - 2V(z)/M)^{1/2}}{(v'^2 - 2V(z)/M)^{1/2}} . \tag{A4}$$

Using Eqs. (A3) and (A4) to eliminate v and $\cos\theta$ in Eq. (A2), we obtain:

$$(v'^2 - 2V(z)/M)^{1/2} = u_m(z) \frac{(v'^2 \cos^2\theta' - 2V(z)/M)^{1/2}}{(v'^2 - 2V(z)/M)^{1/2}} . \tag{A5}$$

In Eq. (A5), $V(z)$ is eliminated by the relation

$$\frac{2V(z)}{M} = u_{m0}^2 - u_m^2(z) .$$

Finally Eqs. (A1) and (A5) are solved for $z = z_{max}$ on the extremum surface in (z, v', θ'), which yields

$$z_{max}(v', \theta') = s \left[1 - \frac{1 - (v'/u_{m0})^2}{\{1 - (v'/u_{m0})^2 (2 - \cos^2\theta')\}^{1/2}} \right] .$$

References

[1] M. J. Kushner, *J. Appl. Phys.* **58**, 4024 (1985).

[2] B. E. Thompson, H. H. Sawin, and D. A. Fisher *J. Appl. Phys.* **63**, 2241 (1988).

[3] J. Pelka, M. Weiss, W. Hoppe, and D. Mewes, *J. Vac. Sci. Technol.* **B 7**, 1483 (1989).

[4] R. T. Farouki, S. Hamaguchi, and M. Dalvie, IBM T. J. Watson Res. Center Report No. 73366 (1991).

[5] W. B. Pennebaker, IBM J. Res. Develop. **23**, 16 (1979).

[6] C. W. Jurgensen, *J. Appl. Phys.* **64**, 590 (1988).

[7] C. W. Jurgensen and E. S. G. Shaqfeh, *J. Appl. Phys.* **64**, 6200 (1988).

[8] S. Hamaguchi, R. T. Farouki, and M. Dalvie, IBM T. J. Watson Res. Center Report No. 73723 (1991).

[9] K.-U. Riemann, U. Ehlemann, and K. Weisemann, *J. Phys. D: Appl. Phys.* **25** 620 (1992).

[10] W. D. Davis and T. A. Vanderslice, *Phys. Rev.* **131**, 219 (1963).

[11] J. Liu, G. L. Huppert, and H. H. Sawin, *J. Appl. Phys.* **68** 3916 (1990).

[12] T. E. Sheridan, and J. Goree, *Phys. Fluids* **B 3**, 2796 (1991).

[13] B. E. Thompson, K. D. Allen, A. D. Richards, and H. H. Sawin, *J. Appl. Phys.* **59**, 1890 (1986).

[14] C. K. Birdsall, *IEEE Trans. Plasma Sci.* **19**, 65 (1991).

[15] V. Vahedi, G. DiPeso, T. D. Rognlien, M. A. Lieberman, and C. K. Birdsall, "Numerical Methods for Modeling Capacitive Discharges and Comparisons with Experiments," to be submitted to *J. Appl. Phys.* (1992).

[16] V. Vahedi, M. A. Leiberman, M. V. Alves, J. P. Verboncoeur, and C. K. Birdsall, *J. Appl. Phys.* **69**, 2008 (1991).

[17] Earl W. McDaniel, *Atomic Collisions*, John Wiley & Sons Inc. (1989).

[18] Birdsall C. K. and A. B. Langdon, *Plasma Physics Via Computer Simulation*, Adam Hilger (1991).

[19] M. A. Lieberman, *J. Appl. Phys.* **65**, 4186 (1989).

List of Figures

List of Tables

case	p [Torr]	V_0 [V]	s [cm]	σ_{cx} [cm^2]	$\sigma_{cx}/\sigma_{scat}$	λ_T/s	$< \theta_1 >$ [D]	$< \theta_T >$ [D]	Γ_y/Γ_z
1	0.001	500	10.0	3×10^{15}	1.5	0.626	18.7	7.47	0.1286
2	0.001	500	10.0	3×10^{15}	6.0	0.894	18.5	2.64	0.0446
3	0.005	500	10.0	3×10^{15}	1.5	0.125	20.0	7.99	0.1376
4	0.005	500	10.0	3×10^{15}	6.0	0.179	19.7	0.32	0.0475
5	0.010	500	10.0	3×10^{15}	6.0	0.089	20.1	2.87	0.0484
6	0.010	500	10.0	3×10^{15}	60.0	0.103	20.0	0.33	0.0055
7	0.010	500	10.0	3×10^{15}	600.0	0.104	20.0	0.03	0.0006
8	0.030	500	10.0	3×10^{15}	6.0	0.030	20.0	2.86	0.0482
9	0.030	500	10.0	3×10^{15}	60.0	0.034	20.0	0.33	0.0055
10	0.030	500	10.0	3×10^{15}	600.0	0.035	20.0	0.03	0.0006
11	0.050	500	10.0	3×10^{15}	6.0	0.018	20.0	2.85	0.0481
12	0.050	500	10.0	3×10^{15}	60.0	0.021	20.0	0.33	0.0055
13	0.050	500	10.0	3×10^{15}	600.0	0.021	20.0	0.03	0.0006
14	0.100	500	10.0	3×10^{15}	6.0	0.009	19.9	2.85	0.0480

Table 1:

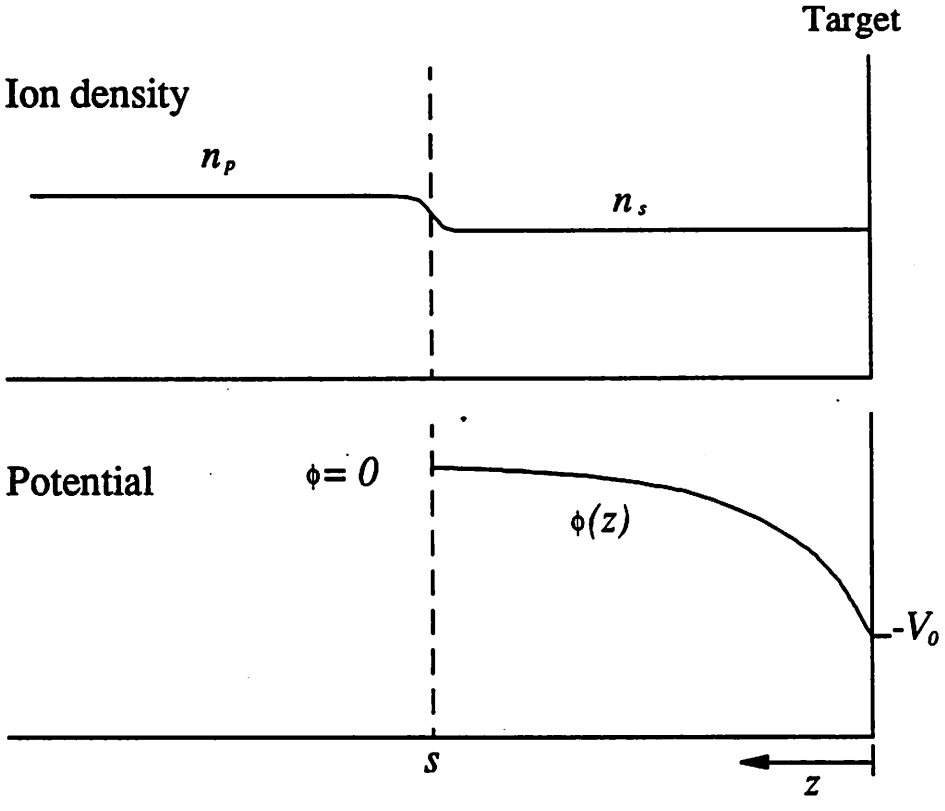

Figure 1:

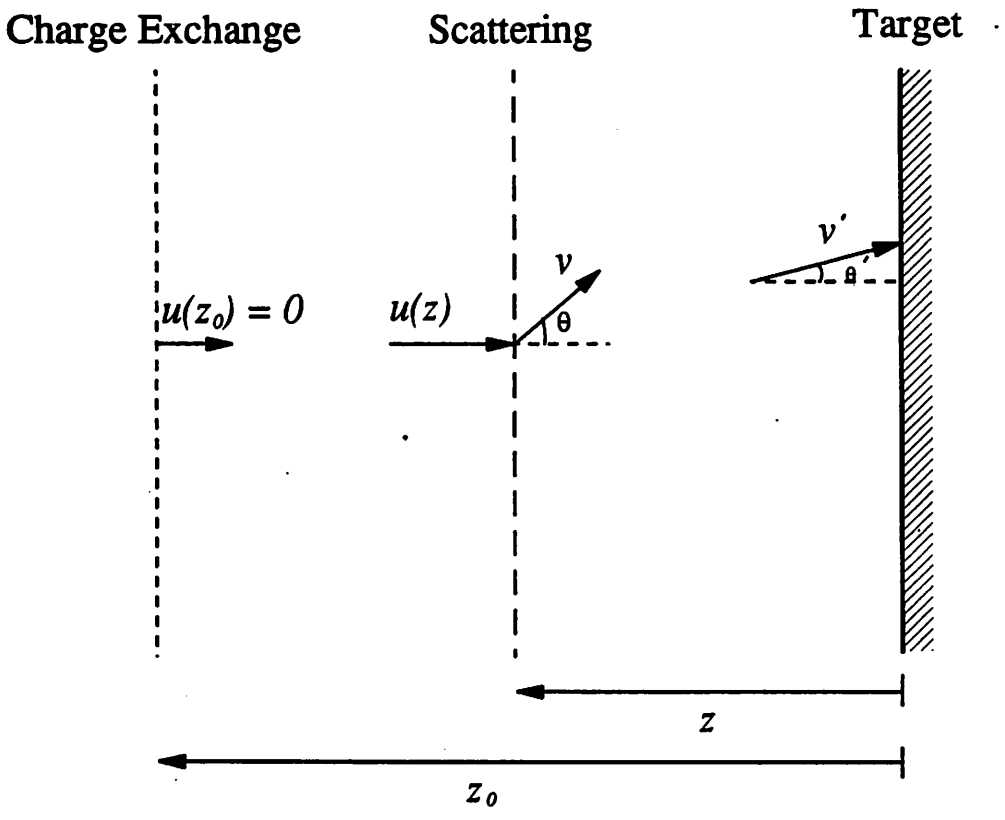
Charge Exchange
Scattering
Target
$u(z_0) = 0$
$u(z)$
v
θ
v'
θ'
z
z_0

Figure 2:

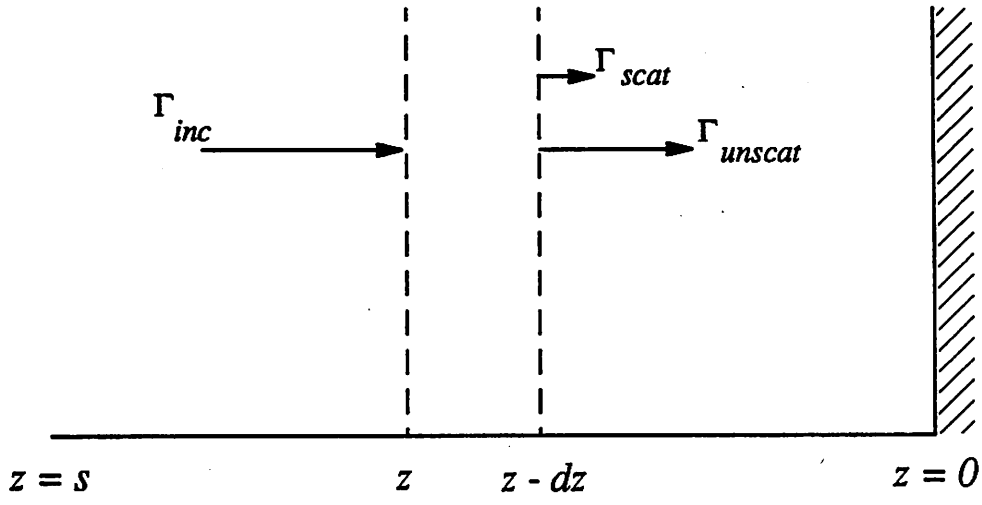

Figure 3:

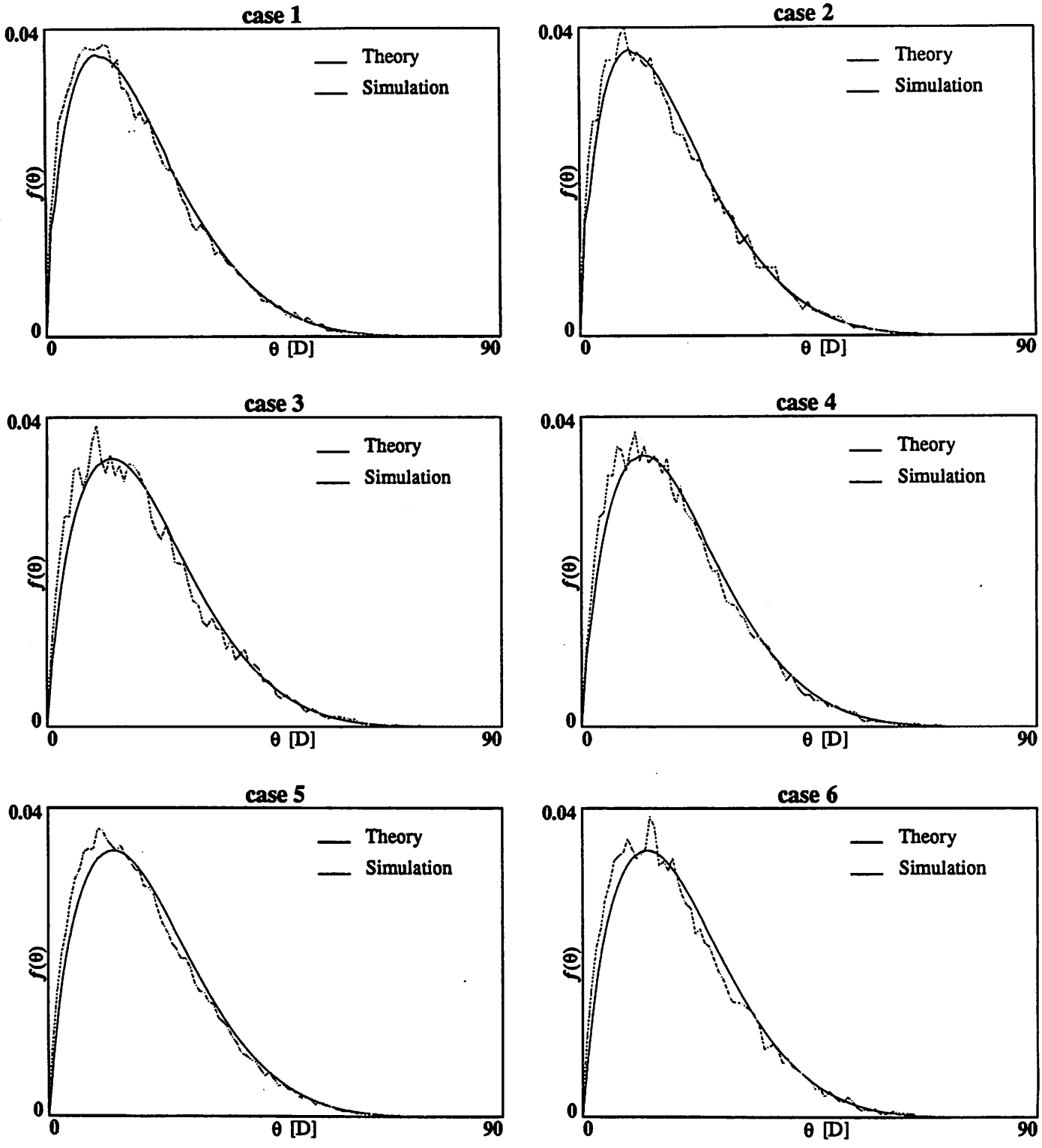
case 1
case 2
case 3
case 4
case 5
case 6
0.04
0
f(θ)
θ [D]
90
Theory
Simulation

Figure 4:

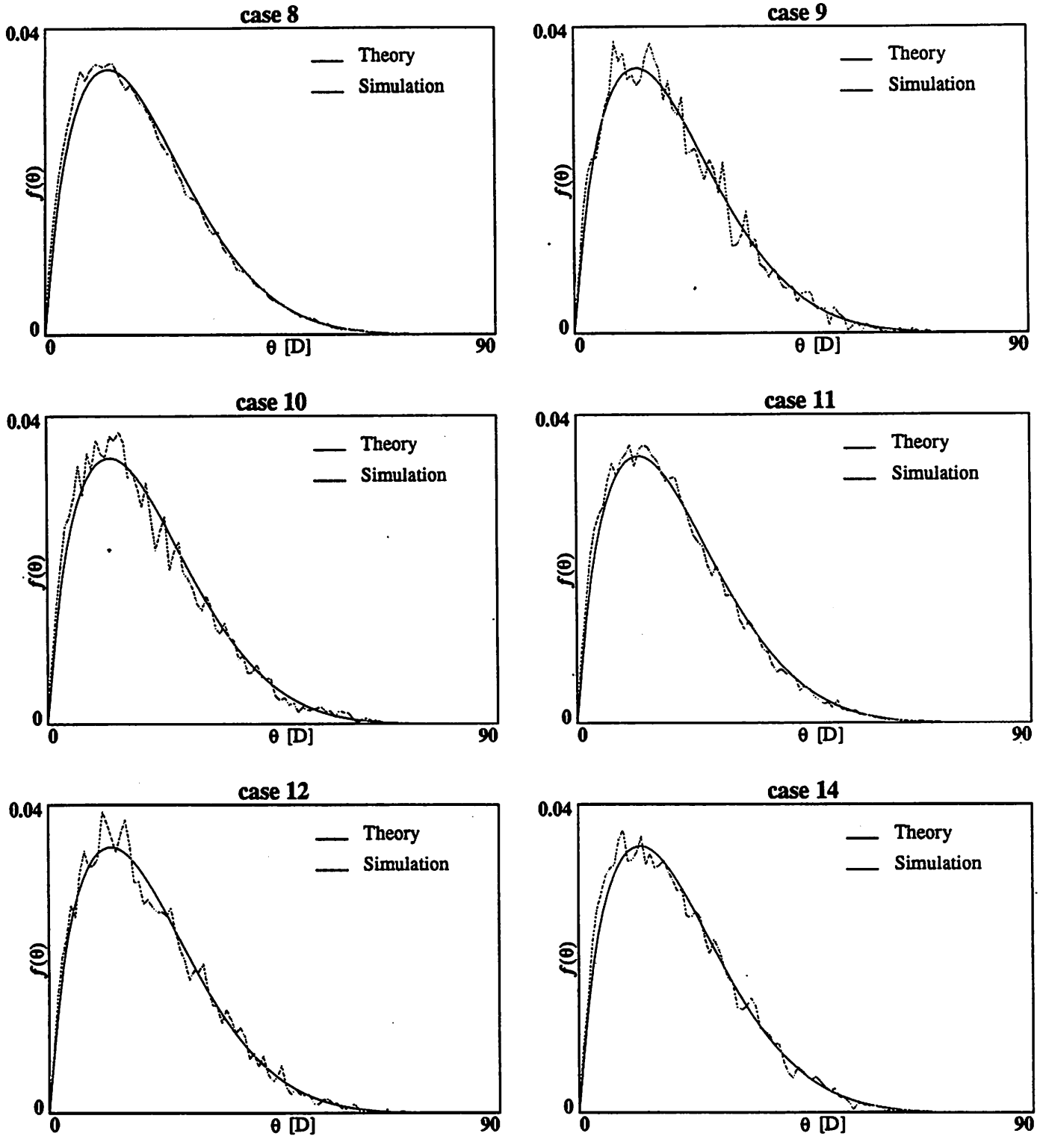
case 8
case 9
case 10
case 11
case 12
case 14
0.04
0
f(θ)
θ [D]
90
Theory
Simulation

Figure 5:

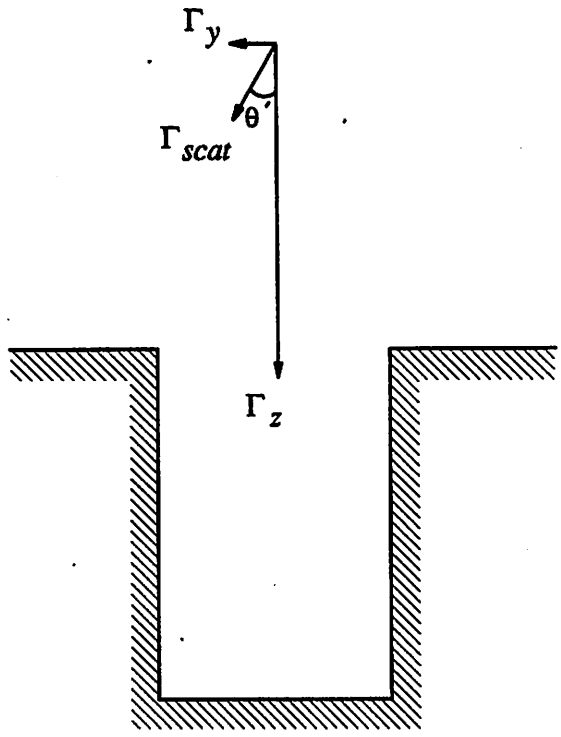

Figure 6: